Flexible and Printed Electronics

Cork derived laser-induced graphene for sustainable green electronics

Flexible and Printed Electronics

PAPER

Cork derived laser-induced graphene for sustainable green electronics

Sara L Silvestre, Tomás Pinheiro, Ana C Marques, Jonas Deuermeier, João Coelho*, Rodrigo Martins, Luís Pereira and Elvira Fortunato

CENIMAT|i3N, Department of Materials Science, School of Science and Technology, NOVA University of Lisbon, and CEMOP/UNINOVA, Caparica, Portugal

* Author to whom any correspondence should be addressed.

E-mail: jcm.coelho@fct.unl.pt

OPEN ACCESS

RECEIVED
11 April 2022

REVISED
11 August 2022

ACCEPTED FOR PUBLICATION
1 September 2022

PUBLISHED
15 September 2022

Keywords: renewable materials, sustainable technology, direct laser writing, cork, laser-induced graphene, micro-supercapacitors

Supplementary material for this article is available online

Abstract

The demand for smart, wearable devices has been dictating our daily life with the evolution of integrated miniaturized electronics. With technological innovations, comes the impactful human footprint left on the planet's ecosystems. Therefore, it is necessary to explore renewable materials and sustainable methodologies for industrial processes. Here, an eco-friendly approach to producing flexible electrodes based on a single-step direct laser writing is reported. A 1.06 μm wavelength fiber laser was used for the first time to produce porous three-dimensional laser-induced graphene (LIG) on an agglomerated cork substrates. The obtained material exhibits the typical Raman spectra, along with an exceptionally low sheet resistance between 7.5 and 10 ohm sq^{-1}. LIG on cork high electrical conductivity and the friendliness of the used production method, makes it an interesting material for future technological applications. To show its applicability, the production of planar micro-supercapacitors was demonstrated, as a proof of concept. Electrochemical performance studies demonstrate that LIG interdigitated electrodes, using PVA-H_2SO_4 electrolyte, achieve an area capacitance of 1.35 mF cm^{-2} (103.63 mF cm^{-3}) at 5 mV s^{-1} and 1.43 mF cm^{-2} (109.62 mF cm^{-3}) at 0.1 mA cm^{-2}. In addition, devices tested under bending conditions exhibit a capacitance of 2.20 mF cm^{-2} (169.22 mF cm^{-3}) at 0.1 mA cm^{-2}. Here, showing that these electrodes can be implemented in energy storage devices, also successfully demonstrating LIG promising application on innovative, green, and self-sustaining platforms.

Abbreviations

MSCs	Micro-supercapacitors
DLW	Direct laser writing
LIG	Laser-induced graphene
cLIG	Cork laser-induced graphene
w-cLIG	Waxed-cork laser-induced graphene
CV	Cyclic voltammetry
GCD	Galvanostatic charge–discharge
SEM	Scanning electron microscopy
EDS	Energy dispersive spectroscopy
XPS	X-ray photoelectron spectroscopy

1. Introduction

Technology has revolutionized and improved our daily lives over the years with the introduction of smart and wearable devices. A multitude of functional materials has been explored in such systems, being graphene one of the most popular for the last couple of years. In fact, it was even recognized with the Physics Nobel Prize in 2010 [1]. Its outstanding physicochemical properties, such as high electrical and thermal conductivity, high surface area, high transmittance, excellent mechanical properties, among others [2], make it a multifaceted and particularly attractive material in several areas [3–5]. Multiple fabrication methods to produce graphene have been explored, which resulted in a one-atom thick layer to multiple layers of carbon [6, 7]. Graphene can as well be functionalized and engineered into a three-dimensional (3D) structure, being suitable for multiple smart technology applications since it allows the necessary features for integration as energy storage devices, sensors, among others [8–10].

Despite the extraordinary advances regarding graphene production and its applications, the ecological footprint of these processes continues to have a significant impact on the environment. Moreover, the most conventional graphene fabrication methods, such as chemical vapor deposition [11, 12] and hydrothermal process of graphene oxide reduction [13–15], are dependent on strictly controlled working conditions, resulting in high costs and poor scalability. A rather promising technique, DLW, exhibits simplicity and a low-cost path to produce multilayer graphene [16]. By using this process, carbon-based materials can be directly and photothermally converted into porous graphene, named LIG [3, 17].

The exploitation of this material has been an intensive research topic, which was already successfully achieved by using different types of lasers, namely ultraviolet [18–20], visible [16, 21], and infrared laser systems [22–24]. Several applications, such as electrochemical sensors, humidity sensors, battery electrodes, electroactuators, supercapacitors, among others were developed [25, 26]. Polymers used for LIG production, such as polyimide, polyetherimide and polysulfone, have been widely reported with very promising results [2, 25, 27]. Nevertheless, the cost and impact on the environment of such polymers to obtain LIG remain a recurring issue. Thus, research on renewable natural materials and strategies to modify its properties is a potential alternative and an open door for a greener technological era. For instance, cellulose-based substrates, such as paper, wood, and cork, converted in LIG are particularly attractive [28–34].

In this work, following the Sustainable Development Goals established by the United Nations, cork, from *Quercus suber* L., being one of nature's most extraordinary and versatile materials in the world, was used as a LIG substrate. Similar to a beehive, cork has cells with pentagonal and hexagonal hollow structures [35, 36], which provides a large surface area to induce porous 3D structures. Furthermore, it presents extraordinary properties, such as lightweight, biodegradability, compressibility, impermeability, resistance to high temperatures, and thermal insulation [37, 38]. Therefore, the possibility of widespread adoption of LIG electrodes in novel flexible and wearable devices could lead to the further development of self-sustainable platforms. Herein, we explore a sustainable production path for eco-friendly technical components, namely electrodes and conductive tracks. By using for the first time, to the best of the author's knowledge, a 1.06 μm wavelength laser to convert cork into LIG (cLIG), promising results were achieved by exploring it as an alternative to a CO_2 laser (10.6 μm wavelength), which is the most used system for LIG preparation. Fiber laser emits radiation near to infrared radiation (IR), which means it works on the same principle as CO_2 laser, inducing thermochemical reactions in the substrate to convert into LIG. However, combining its fast galvo scanning system and photon energy irradiated with meticulously controlling laser parameters, it allows a tunneling of LIG composition, porosity, and morphology [17]. Considering the fiber laser ultra-short duration pulses, it also presents high-resolution patterning, lower thermal degradation, and a high potential for large-scale LIG production [39]. With promising graphitization efficiency in these natural substrates, a proof of concept was developed, with cLIG-based flat MSC successfully produced and characterized.

2. Experimental section

2.1. Synthesis of LIG

Agglomerated cLIG was firstly produced using a 50 W 10.6 μm CO_2 infrared laser (VLS3.5 Laser Platform by Universal Laser Systems, Inc.) and a 50 W 1.06 μm Nd:YAG fiber laser (PLS6MW Multi-wavelength Laser Platform by Universal Laser Systems, Inc.), both equipped with 2.0″ lens. A preliminary study to compare both laser systems were performed by varying laser parameters such as (a) power (adjustable up to 50 W in both lasers), (b) speed (adjustable up to 1.27 m s^{-1} on CO_2 laser and up to 1.78 m s^{-1} on fiber laser), and (c) focal point defocus (from 0.76 mm above focal point to 1.52 mm below). A fixed 1000 pulses per inch was established on the CO_2 laser, and a fixed frequency of 100 kHz was established for the fiber laser. Finally, after all laser parameters optimization, electrodes were produced with fiber laser using 5.5 W, 17.8 mm s^{-1} and 1.52 mm below focal point.

2.2. LIG characterization

LIG was characterized by SEM in a Hitachi TM 3030Plus tabletop workstation to examine the structure, morphology, and cross-section of the produced LIG, while carbon and oxygen content was evaluated by EDS. XPS was performed using a Kratos Axis Supra with monochromated Al Kα and Al Lα sources. The Al Kα source was running at 225 W and detailed scans were recorded with 5 eV pass energy. The Ag Lα source was running at 300 W and the respective detailed scans were recorded with 40 eV pass energy. CasaXPS was used for data analysis. Raman microscopy was carried out with a Renishaw® inViaTM Qontor® confocal Raman microscope equipped with a Renishaw Centrus 2957T3 detector and a 532 nm laser (green) operating at 10 mW. A 50× Olympus objective lens was used to focus the laser beam. All measurements were made with three scans of 10 s laser exposure. For electrical characterization, cLIG was engraved in 5 × 5 mm^2 squares and then silver ink contacts were placed on the ends of the squares. A multimeter was used for preliminary assessments,

followed by resistivity measurements using BioRad HL5500 at room temperature to determine cLIG sheet resistances. cLIG surface wettability was evaluated through contact angle (CA) measurements with Dataphysics OCA15 plus using the sessile drop method. Briefly, 3 μl of electrolyte (H_2SO_4) droplets were placed on the substrate surface and CAs were measured for 15 min, to assess the spreadability of the droplet. The CA analysis was performed with embedded software (SCA 20) using Laplace–Young approximation model with at least three measurements per sample.

2.3. In-plane flexible MSCs fabrication and characterization

For the MSCs development an extra process was added, a pre-treatment of wax to the cork, followed by LIG synthesis and subsequent MSC fabrication/characterization, described below.

2.3.1. Pre-treatment of the agglomerated cork substrate

Agglomerated cork sheets with 2 mm thickness (supplied by Amorim Cork Composites) were pre-treated with a wax-based ink (yellow) from Xerox Limited. Wax was melted on a hot plate at 125 °C for 20 s. After that, cork was placed on top of the melted wax layer, until it was absorbed throughout its volume. Finally, waxed cork was removed from the heating plate and allowed to cool down to room temperature and solidify.

2.3.2. MSCs production and electrochemical characterization

For the in-plane MSCs production in waxed agglomerated cork, Adobe Illustrator software was used for the interdigitated electrodes design. Fixed dimensions were used: lines with 2 mm width and a gap of 0.6 mm between them. Also, two finger pads were defined for the negative and positive electrodes. The w-cLIG based MSCs were tested using aqueous solutions of K_2SO_4 (0.5 M), PVA-H_2SO_4 (1 M) and PVA-H_3PO_4 (1 M) as electrolytes. In a normal procedure, K_2SO_4 electrolyte was produced by dissolving K_2SO_4 (4.35 g) in deionized water (50 ml) under stirring. PVA based electrolytes were prepared by dissolving PVA (1 g) in deionized water (10 ml) at 85 °C under stirring. Once the PVA was dissolved the respective acid (0.5 ml) was added and let under vigorous stirring for 1 h.

The electrochemical performance of the w-cLIG MSC was evaluated by CV at a potential range from 0 to 0.8 V at different scan rates ranging from 5 to 500 mV s^{-1}. GCD tests were carried out at current densities of 0.005, 0.01, 0.02, 0.05 and 0.1 mA cm^{-2}, and a potential window range from 0 to 0.8 V.

All the above electrochemical characterization was performed using PalmSens 4.0 Potentiostat/Galvanostat/Impedance Analyzer (PalmSens Compact Electrochemical Interfaces) at room temperature.

The CV and GCD measurements were used to calculate the areal capacitance (C_A), volumetric capacitance (C_V), areal energy density (E_A) and power density (P_A) of the devices as stated on supporting information.

3. Results and discussion

3.1. cLIG synthesis and characterization

Agglomerated cork sheets were used as the substrate for LIG production. This composite material, made from the agglomeration of natural cork granules with binding agents, results in different size grains being compressed into each other while adhering together. Using agglomerated cork instead of pristine cork brings scalability for industrial use, being currently one of the most marketable materials in the world, allowing the production of multiple substrate shapes, from millimeter sheets to bulky pieces. Also, being a composite material with sophisticated properties can be beneficial for the desired type of application, especially for flexible wearables. Figure 1 shows the substrate morphology, and as expected, coming from a natural source to a processed sheet, different dimensions of granules are observed.

The substrate presents different natural cork granules randomly oriented, and its cellular structure is composed of hexagonal and pentagonal structures as confirmed in the SEM micrographs (figure 1) [32, 40]. It can also be observed that the alveoli walls of the agglomerates are ~1.1 μm thick. The characteristic morphology of the cork is of utter importance, as it enables the production of 3D porous LIG exhibiting high surface area (inside the cork cells and even on the walls). These properties are highly beneficial for electrochemical applications, as they may allow an enhanced charge transfer rate in the LIG electrodes, large available surface area and, consequently, a good energy storage performance [26]. Therefore, the study of cLIG synthesis on this substrate started with a systematic optimization of the laser system, by varying parameters such as power, speed, and focal plane defocus on cork substrate. Regarding the laser wavelength influence, as already reported, infrared lasers mainly result in photothermal conversion, which means that covalent bond breaking occurs by local high temperature induction. Thus, the laser spot size and laser pulse duration influence the LIG formation [41, 42]. These outcomes vary using lasers with different wavelengths, in which a higher resolution laser, such as the fiber laser, reflects in a smaller spot size and a shorter pulse duration than the CO_2 laser [43].

In this work, a fiber laser, with a 1.06 μm wavelength, is reported for the first time, to the best of the author's knowledge, for LIG production on cork. To identify the conditions of power and speed that result in a homogeneous LIG formation, the laser was

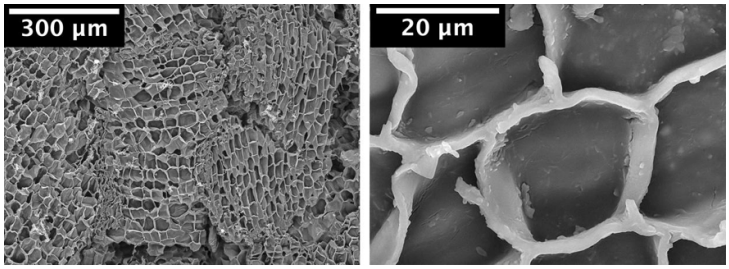

Figure 1. SEM image of the pristine agglomerated cork morphology.

focused on the substrate's surface at its focal point. As reported in the literature, higher laser powers increase LIG thickness, and lower laser speeds result in better quality LIG exhibiting an improved electrical conductivity [24, 31]. It is clear that cork is very sensitive to the variation of the laser conditions since 1% variation in power and speed is enough to promote carbonization or nothing at all, which can be visually inspected in figure S1. The results suggest that laser power cannot be increased too much at lower scanning speed since it results in undesirable outcomes such as laser ablation, thermal damage of the surrounding zones of established pattern, and formation of brittle powder LIG (figure S2(a)). For lower power and higher scanning speed, no changes were visually identified on the substrate or LIG formation did not occur on the entire surface of the defined square. This can be explained by the low energy density delivered to the substrate unable to induce a photothermal conversion [17] (figure S2(b)). After establishing the proper power and speed conditions for fiber laser (5.5 W @ 17.8 mm s^{-1}), a study on the influence of focal point defocus on LIG synthesis was conducted. As reported by Tour *et al* [29], when the laser beam is in a defocused position, the spot size increases, subsequently laser spots overlap, and a multiple lasing effect can be achieved [30]. The multiple lasing method suggests that in some cases LIG formation occurs by two steps: conversion of a carbon precursor into amorphous carbon followed by a conversion to graphene upon subsequent lasing [25, 31]. Using the defocusing method, the process is simplified by only one laser passage, resulting in multiple exposures in the overlapping area [20]. Thus, the effects of defocusing on the characteristics of LIG were explored in this work. The structures obtained by defocusing the laser, from 0.76 mm above and 1.52 mm below the focal plane, were characterized through SEM, as shown in figure S3. Variations in defocusing distances and laser wavelengths result in clearly different LIG morphologies.

These results suggest that cork photothermal conversion into cLIG is in good agreement with the above explanation about the defocusing method. Using the fiber laser at the focal plane ($Z = 0.00$ mm) cork receives a larger amount of energy per unit area, resulting in depth powerful engravings onto the substrate instead of a uniform and continuous carbonization.

By moving the substrate far from the focal plane, in both positive and negative directions of the Z plane, the laser spot size expands over a larger area. This leads to an overlapping of the laser spots with a multiple lasing effect, resulting in better quality LIG [16, 44]. In addition, by defocusing 1.52 mm below the focal point, it produces less depth of focus, and the initial porous honeycomb flake structure of cork (figure 1) prevails even after irradiation (figure S3). Thus, conferring the porous cLIG produced by fiber laser a hexagonal and pentagonal structure with an extensive accessible surface area for posteriorly electrochemical reactions.

Raman spectra of cLIG obtained from fiber laser, show the three prominent peaks of graphitic materials, ranging from 1000 to 3000 cm^{-1}. Two distinctive first-order peaks are presented at ~1350 cm^{-1} (D peak) and ~1580 cm^{-1} (G peak), and a second-order 2D peak is presented at ~2700 cm^{-1}, showing the presence of graphitic carbon [45]. The D band can be related to the formation of defects, vacancies and bent sp^2 bonds, while the G band results from the first-order inelastic scattering process being highly sensitive to the number of layers present in the LIG [46]. The 2D band corresponds to the second-order Raman peak, which results from two photon lattice vibrational process [47]. When relating the SEM images with Raman spectra and sheet resistances, there is a correlation between Raman peaks intensity, the conductivity of the cLIG and structural morphology obtained (figure S4). By defocusing substrate from the focal plane, cLIG samples show a decrease in D peak relative intensity, meaning that fewer defects are induced during LIG conversion, which is in accordance with previously reported works [29, 32].

In terms of sheet resistance, for LIG induced by IR (10.6 μm), visible (450 nm), and UV lasers (355 nm) on cork, there are reported values in the range 46–115 ohm sq^{-1} [32–34]. In the current study using a fiber laser (1.06 μm) with defocusing the distance from the focal plane, cLIG conductivity improves

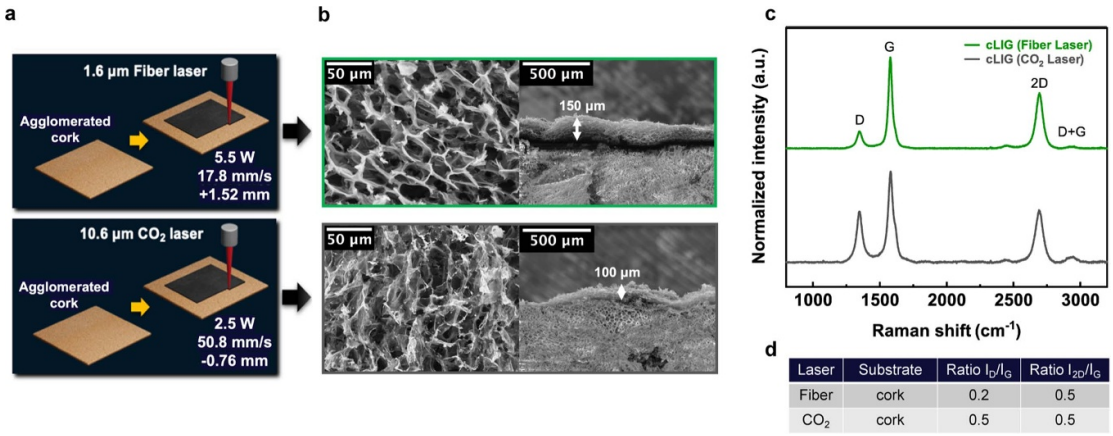

Laser	Substrate	Ratio I_D/I_G	Ratio I_{2D}/I_G
Fiber	cork	0.2	0.5
CO_2	cork	0.5	0.5

Figure 2. (a) Schematic representation of optimized processes for both lasers, (b) SEM micrographs, (c) Raman spectra of the resultant LIG, and (d) table with LIG ratios obtained in Raman spectra.

significantly, showing an incredible enhancement in LIG quality with a sheet resistance almost ten times lower ($R_s \sim 9.86 \pm 0.12$ ohm sq^{-1}). This significant improvement, as already mentioned, is essentially due to the combination and interaction of the type of laser with the substrate used and the laser conditions applied.

XPS was used to characterize cork prior laser irradiation and cLIG conversion, supporting the results above (figure S5). Regarding high-resolution spectrum of the C 1s, cLIG produced revealed the presence of graphene structures. Regarding the variability of the XPS spectra and partial oxidation observed, a factor to be considered is the influence of the place where the measurement is performed. In figure S6 it is shown that in fact the most superficial zones of the sample are more oxidized, while an inner zone results in a LIG with lower oxygen content.

In this work, fiber laser shows its promising application for converting carbon-based materials into LIG, taking advantage of its interaction with the substrate. As CO_2 lasers (with a 10.6 μm wavelength) are the most commonly used systems for LIG conversion on cork substrates [29, 33], a comparison in terms of structural morphology and quality obtained with this system and the fiber laser is described in the supporting information. It was observed that LIG morphology obtained with 10.6 μm CO_2 and 1.06 μm fiber lasers are quite different. In samples produced in the fiber laser a less ablative effect is observed, and better uniformity is achieved, contrarily to the fragile and powdery cLIG microstructure obtained from the CO_2 laser.

A comparison of the optimized laser conditions and resultant LIG properties for both lasers is briefly shown in figure 2. In figures 2(a) and (b) it is visible a significant difference in the LIG morphology produced with different lasers' wavelengths. LIG induced on cork present structures similar to porous and powdery honeycomb flakes, as previously described.

It seems that cLIG produced in the fiber laser is thicker (150 μm), exhibiting a continuous and uniform layer, with a less defective appearance compared to the LIG produced by the CO_2 laser. This can be supported and confirmed with the Raman spectra and ratios from figures 2(c) and (d). As already mentioned, the D peak corresponding essentially to the formation of defects, decreases when switching from the CO_2 to the fiber laser.

It was demonstrated that cLIG quality and the low sheet resistance makes this material attractive for circuit conductive tracks, electrodes, sensors, or even full devices. In the following, and as a proof of concept, w-cLIG electrodes prepared at optimized conditions were tested as a flexible and sustainable MSC.

3.2. Proof-of-concept in-plane MSC fabrication and characterization

After the optimization process, cLIG was used to design interdigitated electrodes for MSC applications. However, during MSC preparation it was verified a random spreading when the electrolyte was drop-casted onto the MSCs' active area. Hence, there was no control in defining the active area where the electrolyte should be deposited nor was it guaranteed that the electrolyte dried on the substrate surface where the electrodes were engraved. Consequently, a proper assessment of the device electrochemical properties was not possible. To circumvent this issue, a wax-based pre-treatment on cork was performed. The wax-based ink can be absorbed throughout the entire cork bulk volume when heated, occupying the free spaces between the granules. In the supporting information is described a brief characterization of the cLIG induced into waxed-cork substrate (figure S7).

CAs of untreated and post-treated substrate surfaces were measured before laser irradiation, to assess wettability of different surfaces over time (table S1). The wax pre-treatment on cork resulted

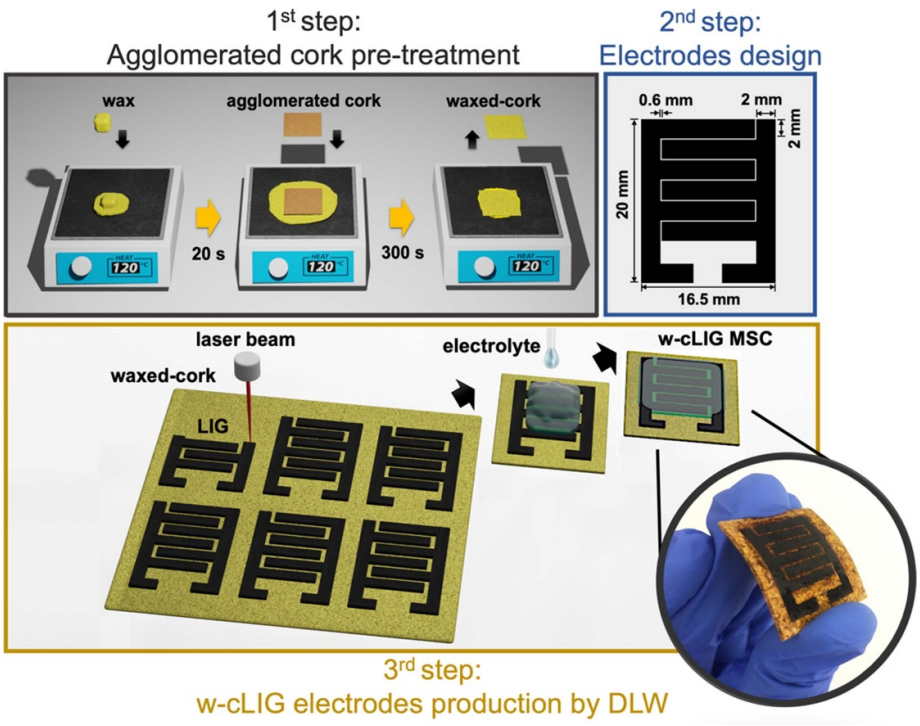

Figure 3. Schematic representation of the w-cLIG-MSC fabrication: 1st step—agglomerated cork pre-treatment, 2nd step—electrode design, and 3rd step—production of the flexible w-cLIG MSC by DLW technique. Finally, electrolyte deposition was taken.

in a hydrophobic interaction between electrolyte and surface of the LIG/substrate, solving the uncontrolled spread of the electrolyte. Furthermore, compared with untreated substrate, only a minimal reduction in sheet resistance was observed with an R_s of approximately 7.5 ohm sq^{-1} (figure S8), proving that this step is not relevant for conductivity improvement but an important approach for MSC assembly. The possibility of maintaining good properties of LIG and improving other aspects such as the surface wettability and adhesion, makes this treatment very innovative and promising.

After this process, MSC electrodes based on w-cLIG were patterned and integrated in flexible MSCs. A schematic representation of the MSC fabrication process is shown in figure 3.

For the electrochemical performance assessment, w-cLIG flexible MSCs were fabricated and tested using different electrolytes. Comparison of the correspondent areal and volumetric capacitances in function of scan rate (from 5 to 500 mV s^{-1}), obtained from CV curves are shown in figure S9. Although using the same electrode dimensions for all the MSCs produced, different CV curves were obtained suggesting different electrolyte-LIG electrodes interaction. By increasing the scan rates, 'quasi-rectangular' to a 'fish' shape curves are identified for all devices produced, which is more prominent on w-cLIG MSCs with PVA-H_2SO_4. This electrolyte is well-known to remain a viscous gel with an apparent higher water content upon drying, which enhances the electrochemical performance for graphene based MSCs [48, 49]. Since the PVA-H_2SO_4 electrolyte rendered w-cLIG MSC the best electrochemical performance among the tested electrolytes, further characterization is shown in figure 4. The GCD curves of the MSC at different current densities of 0.005, 0.01, 0.02, 0.05 and 0.1 mA cm^{-2} were measured to determine the electrochemical performance of the device over time (figure 4(b)).

Pseudosymmetrical response curves were observed, which mean that its potential changes linearly with time due to its stable and reversible properties.

In figures 4(c), a gradual decrease in MSCs capacitance is observed with the scan rate, where the maximum areal capacitance (C_A) reached was 1.35 mF cm^{-2} (with a corresponding C_V of 103.63 mF cm^{-3} for w-cLIG with 130 μm of thickness) at a scan rate of 5 mV s^{-1}, respectively.

This phenomenon can be explained by the ion diffusion mechanisms in the LIG-MSCs. At lower scan rates, electrolyte ions have more time to move and to penetrate deeply into the available pores in the LIG structure, which results in a higher areal capacitance [50]. At higher scan rates, a loss of efficiency of ions to infiltrate the LIG occurs, leading to a reduction on capacitance [51–53]. Therefore, figure 4(d) shows the capacitance retention of the MSCs using PVA-H_2SO_4, which confirmed device excellent stability after 10 000 cycles at a current density of 0.05 mA cm^{-2}. During the cyclability test, it

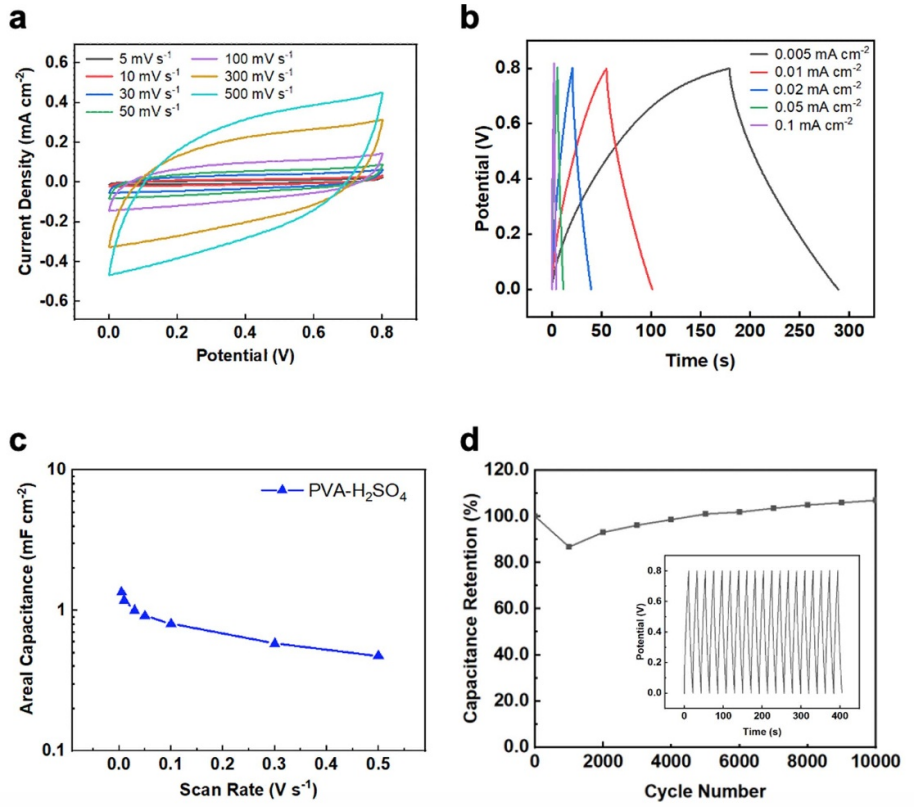

Figure 4. Electrochemical characterization of a w-cLIG MSC using PVA-H_2SO_4 electrolyte. (a) Cyclic voltammograms measured at different scan rates (in the 5–500 mV s^{-1} interval). (b) Galvanostatic charge and discharge (GCD) curve of the device with a current density of 0.005, 0.01, 0.02, 0.05 and 0.1 mA cm^{-2}. (c) Areal and volumetric capacitances in function of scan rate obtained from CV curves. (d) Capacitance retention versus cycle number obtained from CGD curves at a current density of 0.05 mA cm^{-2}. Insets: representative GCD curves of the first cyclability for the same MSC.

was observed a slight increase in capacitance retention with a tendency to stabilize over operation time like already reported [54]. A loss of MSC capacity is observed mostly due to parasitic irreversible electrochemical reactions that occur in the first phase of the cyclability test. Over a number of cycles, the electrodes adapt, and the pores open within its structure. This enhances the wettability of the electrolyte within the LIG structure, promoting greater activation of the ionic diffusion paths and electrochemical reactions. Also, unwanted species of the electrolyte are consumed over a larger number of cycles, tending to increase the supercapacitor capacity until it becomes stable. Therefore, throughout the charge and discharge process of the device, a gradual increase of the capacitance retention is observed. This is not a common electrode behavior, however it was already observed in other nanomaterials based systems [55]. For this reason, w-cLIG electrodes exhibit long-term cyclical stability, which proves to be an excellent material with promising functionality in MSC applications.

To study the flexibility of the device and corresponding electrochemical performance, bending tests were carried out as presented in figure 5. Comparing the flat and bent MSC (with 35° angle), an increase in charge–discharge time in the GCD curve is observed. This behavior can be related with the deformation submitted to its structure and an opening of the spongy pores, which suggests an enhancing of the charge storage performance with expansion of the active area [56]. Also, when the MSC is bent, it benefits from the infiltration of the electrolyte through longer paths leading to a better charge carrier distribution.

In figures 5(c) and (d), the areal and volumetric capacitances were plotted at different current densities, calculated from the GCD curves using equations (3) and (4) from supporting information.

Flat conformation yields a C_A of 1.43 mF cm^{-2} at 0.1 mA cm^{-2} (C_V corresponding to 109.62 mF cm^{-3}) and bent MSC resulted on a C_A of 2.20 mF cm^{-2} at 0.1 mA cm^{-2} (C_V corresponding to 169.23 mF cm^{-3}). These values confirm the suggestions above, where it was mentioned that a bent conformation increases LIG paths and facilitate ionic diffusion, consequently yielding a better capacitance.

In addition, areal and volumetric energy, and power densities of the flat and bent MSCs were evaluated, and the Ragone plots are shown in figure 6. Greater areal and volumetric capacitances obtained with the bent MSC reflects in better energy-power characteristics, which is in accordance with results demonstrated above. Flat w-cLIG MSC exhibits an

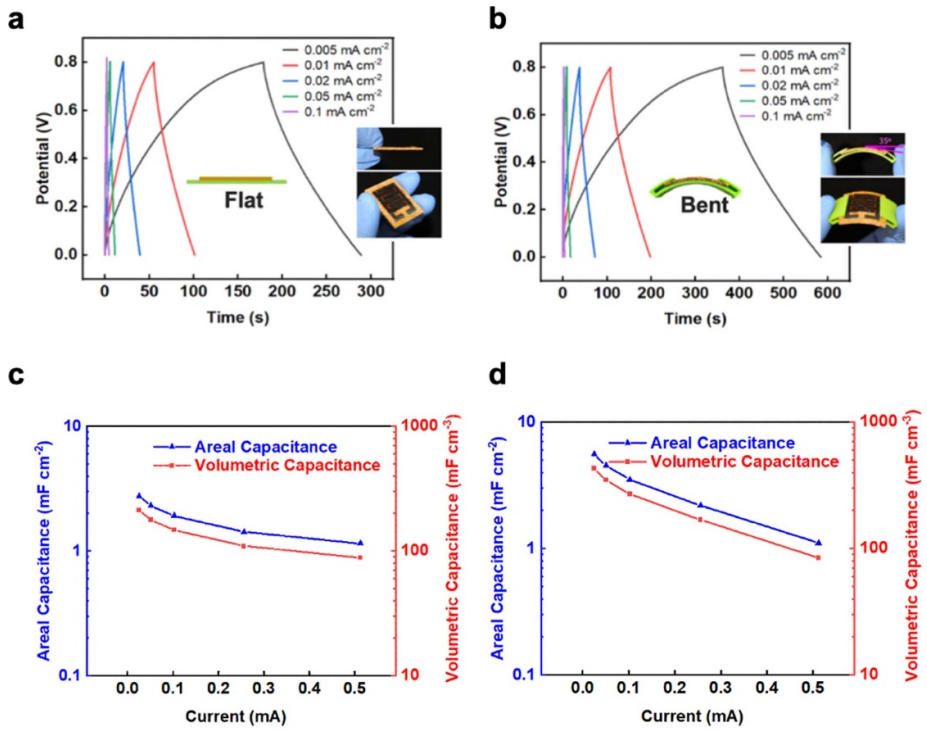

Figure 5. The galvanostatic charge and discharge (GCD) curve of (a) flat and (b) bent w-cLIG MSC with a current density of 0.005, 0.01, 0.02, 0.05 and 0.1 mA cm^{-2}. GCD curve comparison of (c) flat and (d) bent w-cLIG MSC areal and volumetric capacitance calculated from GCD data.

E_A of 0.13 μWh cm^{-2} and an E_V of 9.74 μWh cm^{-3} at the current density of 0.1 mA cm^{-2}. For the bent conformation, the MSC was able to deliver the highest E_A of 0.20 μWh cm^{-2} and an E_V of 15.04 μWh cm^{-3} at the same current value. The areal power densities resulting from flat and bent conformation reached 80 μW cm^{-2} and a corresponding P_V of 6154 μW cm^{-3} at the same current value.

By focusing this work on the sustainability and simplicity of the processes used, it is shown that exploring the use of renewable materials to develop electronics can achieve equally good or even better performances than what is currently found in the literature (table 1). Similar works have already reported the conversion of natural carbon substrates into LIG electrodes, using laser sources ranging from UV to IR wavelengths. Thus, the properties of LIG can be manipulated according to each target application, achieving tailored electrical, physical, chemical resistance, and structural properties. However, different substrates can have limitations in terms of compatibility radiation absorption for specific wavelength lasers. This work introduces the importance of exploring the application of an alternative laser source (fiber) for LIG synthesis in an agglomerated cork, without the need to use doping strategies or pre-treatments on the substrate. In contrast with that, the properties of the electrodes vary and, a porous w-cLIG with excellent properties was achieved with greater conductivity and fewer defects. Also, the optimized laser conditions, the electrodes design/geometry can also influence LIG properties. Overall, LIG electrodes induced on cork substrates with a fiber laser have the potential for low-cost MSCs electrodes fabrication compared to previous LIG reports produced on natural substrates by DLW, with similar electrochemical performances. It is important to highlight the fact that different lasers used on similar substrates do not always achieve the same results and therefore, the obtain metrics and consequent comparisons are not always straightforward.

MSC development on cork substrates is just one example of one possible application for LIG. It holds a great potential for future technology not only due to the simplicity of optimizing the electrodes but also due to the intrinsic properties of the substrate itself. Additionally, these metrics can be translated to other systems, such as transistors, sensors and general circuitry or conductive paths. Additionaly, it is still possible to explore multiple lasing and doping strategies and other pre-treatments to the cork substrate to obtain better quality LIG, with enhanced properties adapted to the desired application. With this work, it is shown that LIG is to be a good candidate for further technological advances in electronics, due to its low sheet resistance, adaptability, low cost, and simplicity.

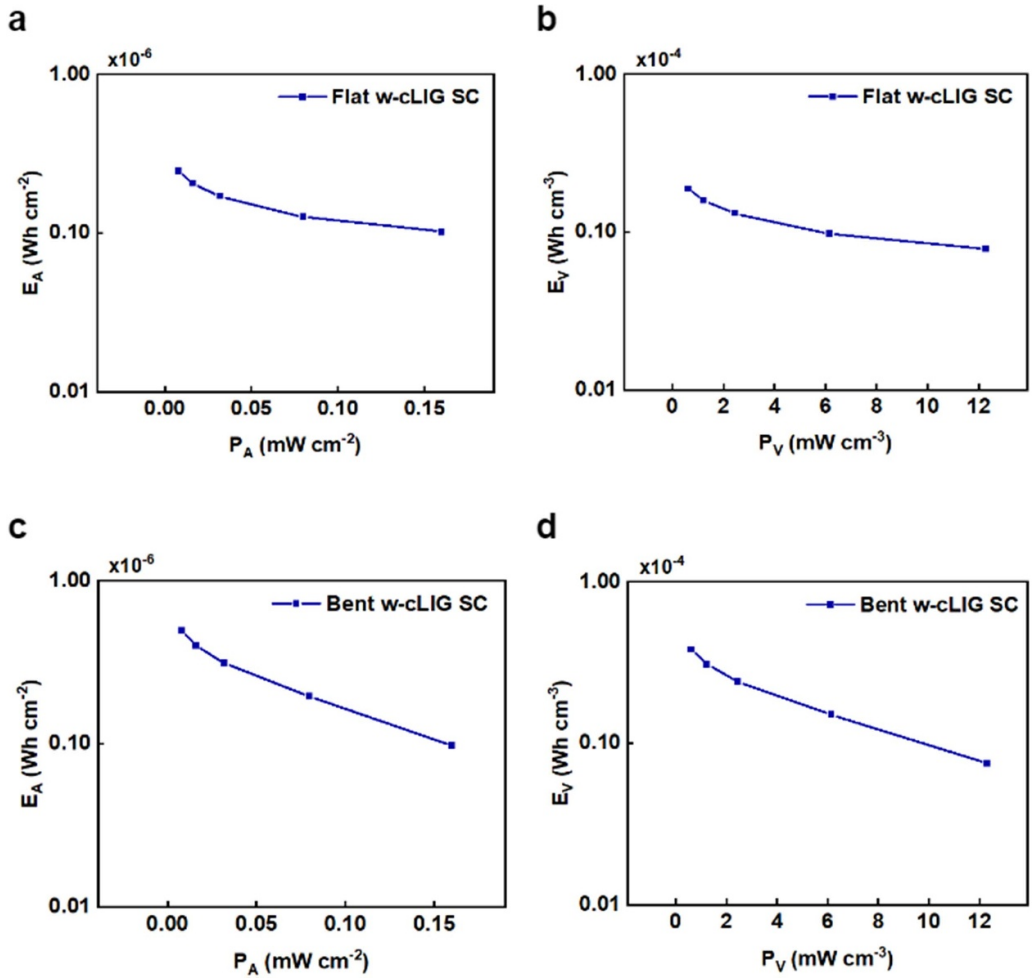

Figure 6. Ragone plots of w-cLIG MSCs (a) areal and (b) volumetric energy densities in flat conformation, and (c) areal and (d) volumetric energy densities in bent conformation.

Table 1. Comparison of planar LIG-based flexible MSCs capacitances from literature, using DLW methods on natural substrates.

Electrode	Laser	Electrolyte	Capacitance	Capacitance retention	References
LIG/waxed cork	1.06 μm NIR (fiber)	PVA-H_2SO_4	1.35 mF cm^{-2} @ 5 mV s^{-1} 1.43 mF cm^{-2} @ 0.1 mA cm^{-2}	106% (>10 000 cycles @ 0.05 mA cm^{-2})	This work
LIG/natural cork	450 nm UV	PVA-H_2SO_4	1.56 mF cm^{-2} @ 0.1 mA cm^{-2}	99.7% (>5000 cycles @ 0.1 mA cm^{-2})	[34]
LIG/kraft lignin	10.6 μm IR (CO_2)	PVA-H_2SO_4	0.88 mF cm^{-2} @ 10 mV s^{-1}	91% (>10 000 cycles @ 0.02 mA cm^{-2})	[50]
LIG/phenolic resin	405 nm UV	—	0.78 mF cm^{-2} @ 500 mV s^{-1}	93.8% (>2000 cycles @ 1 mA cm^{-2})	[56]
LIG/wood	10.6 μm IR (CO_2)	PVA-H_2SO_4	1 mF cm^{-2} @ 1 mA cm^{-2}	—	[57]

4. Conclusion

This work has successfully demonstrated a simple, eco-friendly and efficient path for the fabrication of LIG electrodes using cork, a renewable substrate. The LIG structure was induced and controlled by a DLW technique, a one-step, maskless, scalable and cost-effective process. A systematic characterization of the LIG induced on untreated agglomerated cork was investigated. Therefore, using a fiber laser on cork substrate with tuned conditions of 5.5 W, 17.8 mm s^{-1} and a laser distance of 1.52 mm below

the focal point, resulted in the best LIG characteristics in terms of morphology, structure, conductivity, and quality. Additionally, for a MSC proof-of-concept, a pre-treatment with wax-based ink on cork led to a controlled deposition of electrolyte on the substrate, without the need for mechanical masks and complex processes. Thus, w-cLIG electrodes were produced using the optimized conditions already established with untreated cork substrate, and showed great characteristics for MSC fabrication with an excellent sheet resistance of approximately 7.5 ohm sq^{-1}. The device was compared with other reports and showed an areal capacitance of 1.35 mF cm^{-2} at 5 mV s^{-1} and 1.43 mF cm^{-2} at 1 mA cm^{-2}. Finally, the electrochemical performance of the w-cLIG electrodes is shown to render a great performance to fulfill the requirements for flexible energy storage devices to multiple other applications, which may hold great interest in future improvements. It was proved that it is possible to join sustainable materials and low-cost techniques for LIG electrodes production, representing a mandatory step for a clean and green future in wearable and self-sustainable electronics.

Author Contributions

Sara L Silvestre: Conceptualization, Methodology, Writing—Original draft preparation, Formal analysis, Investigation. Tomas Pinheiro: Writing—Review and Editing. Ana C Marques: Writing—Review and Editing. Jonas Deuermeier: Review and Editing. João Coelho: Validation, Supervision, Writing—Review and Editing. Rodrigo Martins: Review and Editing, Funding acquisition. Luís Pereira: Validation, Supervision, Writing—Review and Editing, Funding acquisition. Elvira Fortunato: Conceptualization, Validation, Supervision, Writing—Review and Editing, Funding acquisition.

The manuscript was written through contributions of all authors. All authors have given approval to the final version of the manuscript.

Data availability statement

All data that support the findings of this study are included within the article (and any supplementary files).

Acknowledgments

This work was financed by national funds from FCT—Fundação para a Ciência e a Tecnologia, I P, in the scope of the projects LA/P/0037/2020, UIDP/50025/2020 and UIDB/50025/2020 of the Associate Laboratory Institute of Nanostructures, Nanomodelling and Nanofabrication—i3N. The authors acknowledge the ERC AdG Grant 787410 from the Project DIGISMART, EC Project SYNERGY H2020-WIDESPREAD-2020-5, CSA, Proposal Number 952169, and Project FOXES, FETPROACT-EIC-05-2019—FET Proactive, Proposal Number 951774. S L Silvestre, T Pinheiro and A C Marques acknowledge PhD grant SFRH/BD/149751/2019, SFRH/BD/08606/2020 and SFRH/BD/115173/2016, respectively. The authors thank Amorim Cork Composites for providing the cork samples used in this work.

ORCID iDs

Sara L Silvestre https://orcid.org/0000-0003-3560-4317
Tomás Pinheiro https://orcid.org/0000-0002-8346-4198
Ana C Marques https://orcid.org/0000-0001-6878-1040
Jonas Deuermeier https://orcid.org/0000-0002-2764-3124
João Coelho https://orcid.org/0000-0003-4217-3842
Rodrigo Martins https://orcid.org/0000-0002-1997-7669
Luís Pereira https://orcid.org/0000-0001-8281-8663
Elvira Fortunato https://orcid.org/0000-0002-4202-7047

References

[1] Geim A K 2012 Graphene prehistory *Phys. Scr.* **T146** 014003
[2] Vivaldi F M, Dallinger A, Bonini A, Poma N, Sembranti L, Biagini D, Salvo P, Greco F and Di Francesco F 2021 Three-dimensional (3D) laser-induced graphene: structure, properties, and application to chemical sensing *ACS Appl. Mater. Interfaces* **13** 30245–60
[3] Thamaraiselvan C, Wang J, James D K, Narkhede P, Singh S P, Jassby D, Tour J M and Arnusch C J 2020 Laser-induced graphene and carbon nanotubes as conductive carbon-based materials in environmental technology *Mater. Today* **34** 115–31
[4] Huang H *et al* 2020 The chemistry and promising applications of graphene and porous graphene materials *Adv. Funct. Mater.* **30** 1–39
[5] Zhu J, Huang X and Song W 2021 Physical and chemical sensors on the basis of laser-induced graphene: mechanisms, applications, and perspectives *ACS Nano* **15** 18708–41
[6] Tiwari S K, Sahoo S, Wang N and Huczko A 2020 Graphene research and their outputs: status and prospect *J. Sci. Adv. Mater. Devices* **5** 10–29
[7] Ma R, Zhou Y, Bi H, Yang M, Wang J, Liu Q and Huang F 2020 Multidimensional graphene structures and beyond: unique properties, syntheses and applications *Prog. Mater. Sci.* **113** 100665
[8] Zheng Q, Lee J, Shen X, Chen X and Kim J-K 2020 Graphene-based wearable piezoresistive physical sensors *Mater. Today* **36** 158–79
[9] Ma Y, Chen J, Hu Y, Zhang Y, Zhang Z, Zhan J, Chen A and Peng Q 2020 Synthesis of three-dimensional graphene-based materials for applications in energy storage *JOM* **72** 2445–59
[10] Dhinakaran V, Lavanya M, Vigneswari K, Ravichandran M and Vijayakumar M D 2020 Review on exploration of graphene in diverse applications and its future horizon *Mater. Today Proc.* **27** 824–8

[11] Chen K, Shi L, Zhang Y and Liu Z 2018 Scalable chemical-vapour-deposition growth of three-dimensional graphene materials towards energy-related applications *Chem. Soc. Rev.* **47** 3018–36
[12] Plutnar J, Pumera M and Sofer Z 2018 The chemistry of CVD graphene *J. Mater. Chem.* C **6** 6082–101
[13] Agarwal V and Zetterlund P B 2021 Strategies for reduction of graphene oxide—a comprehensive review *Chem. Eng. J.* **405** 127018
[14] Huang H H, De Silva K K H, Kumara G R A and Yoshimura M 2018 Structural evolution of hydrothermally derived reduced graphene oxide *Sci. Rep.* **8** 2–10
[15] Tian Y, Yu Z, Cao L, Zhang X L, Sun C and Wang D W 2021 Graphene oxide: an emerging electromaterial for energy storage and conversion *J. Energy Chem.* **55** 323–44
[16] Stanford M G, Zhang C, Fowlkes J D, Hoffman A, Ivanov I N, Rack P D and Tour J M 2020 High-resolution laser-induced graphene. Flexible electronics beyond the visible limit *ACS Appl. Mater. Interfaces* **12** 10902–7
[17] Ye R, James D K and Tour J M 2019 Laser-induced graphene: from discovery to translation *Adv. Mater.* **31** 1–15
[18] Carvalho A F, Fernandes A J S, Leitão C, Deuermeier J, Marques A C, Martins R, Fortunato E and Costa F M 2018 Laser-induced graphene strain sensors produced by ultraviolet irradiation of polyimide *Adv. Funct. Mater.* **28** 1805271
[19] Chen Y, Long J, Zhou S, Shi D, Huang Y, Chen X, Gao J, Zhao N and Wong C P 2019 UV laser-induced polyimide-to-graphene conversion: modeling, fabrication, and application *Small Methods* **3** 1–9
[20] Kulyk B, Silva B F R, Carvalho A F, Barbosa P, Girão A V, Deuermeier J, Fernandes A J S, Figueiredo F M L, Fortunato E and Costa F M 2022 Laser-induced graphene from paper by ultraviolet irradiation: humidity and temperature sensors *Adv. Mater. Technol.* **7** 2101311
[21] Burke M, Larrigy C, Vaughan E, Paterakis G, Sygellou L, Quinn A J, Herzog G, Galiotis C and Iacopino D 2020 Fabrication and electrochemical properties of three-dimensional (3D) porous graphitic and graphenelike electrodes obtained by low-cost direct laser writing methods *ACS Omega* **5** 1540–8
[22] Lin J, Peng Z, Liu Y, Ruiz-Zepeda F, Ye R, Samuel E L G, Yacaman M J, Yakobson B I and Tour J M 2014 Laser-induced porous graphene films from commercial polymers *Nat. Commun.* **5** 5714
[23] Romero F J, Gerardo D, Romero R, Ortiz-Gomez I, Salinas-Castillo A, Moraila-Martinez C L, Rodriguez N and Morales D P 2020 Comparison of laser-synthetized nanographene-based electrodes for flexible supercapacitors *Micromachines* **11** 555
[24] Samouco A, Marques A C, Pimentel A, Martins R and Fortunato E 2018 Laser-induced electrodes towards low-cost flexible UV ZnO sensors *Flex. Print. Electron.* **3** 0–21
[25] Huang L, Su J, Song Y and Ye R 2020 Laser-induced graphene: en route to smart sensing *Nano-Micro Lett.* **12** 157
[26] Li G 2020 Direct laser writing of graphene electrodes *J. Phys. D: Appl. Phys.* **127** 010901
[27] Han T, Nag A, Afsarimanesh N, Mukhopadhyay S C, Kundu S and Xu Y 2019 Laser-assisted printed flexible sensors: a review *Sensors* **19** 1462
[28] Le T S D, Park S, An J, Lee P S and Kim Y J 2019 Ultrafast laser pulses enable one-step graphene patterning on woods and leaves for green electronics *Adv. Funct. Mater.* **29** 1–10
[29] Tour J M, Li Y, Ye R, Chyan Y, Arnusch C J and Singh S P 2018 Laser-induced graphene by multiple lasing: toward electronics on cloth, paper, and food *ACS Nano* **12** 2176–83
[30] Kulyk B, Silva B, Carvalho A, Silvestre S, Fernandes A, Martins R, Fortunato E and Costa F 2021 Laser-induced graphene from paper for mechanical sensing *ACS Appl. Mater. Interfaces* **13** 10210–21
[31] Pinheiro T, Silvestre S, Coelho J, Marques A C, Martins R, Sales M G F and Fortunato E 2021 Laser-induced graphene on paper toward efficient fabrication of flexible, planar electrodes for electrochemical sensing *Adv. Mater. Interfaces* **8** 2101502
[32] Carvalho A F, Fernandes A J S, Martins R, Fortunato E and Costa F M 2020 Laser-induced graphene piezoresistive sensors synthesized directly on cork insoles for gait analysis *Adv. Mater. Technol.* **5** 1–8
[33] Stanford M G, Li J T, Chyan Y, Wang Z, Wang W and Tour J M 2019 Laser-induced graphene triboelectric nanogenerators *ACS Nano* **13** 7166–74
[34] Imbrogno A *et al* 2022 Laser-induced graphene supercapacitors by direct laser writing of cork natural substrates *ACS Appl. Electron. Mater.* **4** 1c01202
[35] Pereira H, Rosa M E and Fortes M A 1987 The cellular structure of cork from *Quercus suber* L. *IAWA J.* **8** 213–8
[36] Duarte A P and Bordado J C 2015 Cork—a renewable raw material: forecast of industrial potential and development priorities *Front. Mater.* **2** 1–8
[37] Silva S P, Sabino M A, Fernandes E M, Correlo V M, Boesel L F and Reis R L 2005 Cork: properties, capabilities and applications *Int. Mater. Rev.* **50** 345–65
[38] Costa A, Barbosa I, Miguel C and Graça J 2021 Variation of cork porosity along the stem in harvested cork oak (*Quercus suber* L.) trees *Ann. For. Sci.* **78** 52
[39] Luong D X *et al* 2018 Laminated object manufacturing of 3D-printed laser-induced graphene foams *Adv. Mater.* **30** 1707416
[40] Lagorce-tachon A *et al* 2015 The cork viewed from the inside *J. Food Eng.* **149** 214–21
[41] Wang X and Zhang Q 2020 Recent progress on laser fabrication of on-chip microsupercapacitors *J. Energy Storage* **34** 101994
[42] Wang L, Wang Z and Bakhtiyari A N 2020 A comparative study of laser-induced graphene by CO_2 infrared laser and 355 nm ultraviolet (UV) laser *Micromachines* **11** 1094
[43] Mamleyev E R, Kudryashov V V, Heissler S, Länge K, Nefedov A, Nordin N, MacKinnon N, Sharma S and Weidler P G 2018 Laser-induced hierarchical carbon patterns on polyimide substrates for flexible urea sensors *npj Flex. Electron.* **3** 2
[44] Choi K H, Park S, Hyeong S K, Bae S, Hong J M, Kim T W, Lee S H, Ryu S and Lee S K 2020 Triboelectric effect of surface morphology controlled laser induced graphene *J. Mater. Chem.* A **8** 19822–32
[45] Mendes L F, de Siervo A, Reis de Araujo W and Longo Cesar Paixão T R 2020 Reagentless fabrication of a porous graphene-like electrochemical device from phenolic paper using laser-scribing *Carbon* **159** 110–8
[46] Chen B *et al* 2021 Tuning the structure, conductivity, and wettability of laser-induced graphene for multiplexed open microfluidic environmental biosensing and energy storage devices *ACS Nano* **16** 15–28
[47] Wall M 2011 The Raman Spectroscopy of Graphene and the Determination of Layer Thickness
[48] Singh R and Charu Tripathi C 2018 Study of graphene based flexible supercapacitors with different gel electrolytes *Mater. Today Proc.* **5** 943–9
[49] Chen Q, Li X, Zang X, Cao Y, He Y, Li P, Wang K, Wei J, Wu D and Zhu H 2014 Effect of different gel electrolytes on graphene-based solid-state supercapacitors *RSC Adv.* **4** 36253–6
[50] Mahmood F, Mahmood F, Zhang H, Lin J and Wan C 2020 Laser-induced graphene derived from kraft lignin for flexible supercapacitors *ACS Omega* **5** 14611–8
[51] Li T, Cao Y, Xue W, Sun B and Zhu D 2020 Self-assembly of graphene-based planar micro-supercapacitor with selective laser etching-induced superhydrophobic/superhydrophilic pattern *SN Appl. Sci.* **2** 206

[52] Liang J, Mondal A K, Wang D and Iacopi F 2019 Graphene-based planar microsupercapacitors : recent advances and future challenges *Adv Mater. Technol.* **4** 1800200
[53] Bu F, Zhou W, Xu Y, Du Y and Guan C 2020 Recent developments of advanced micro-supercapacitors design, fabrication and applications *npj Flex. Electron.* **4** 31
[54] Gul H, Shah A U H A and Bilal S 2019 Achieving ultrahigh cycling stability and extended potential window for supercapacitors through asymmetric combination of conductive polymer nanocomposite and activated carbon *Polymers* **11** 1678
[55] Zhang C J *et al* 2020 Extra lithium-ion storage capacity enabled by liquid-phase exfoliated indium selenide nanosheets conductive network *Energy Environ. Sci.* **13** 2124–33
[56] Yun X, Xiong Z, Tu L, Bai L and Wang X 2017 Hierarchical porous graphene film: an ideal material for laser-carving fabrication of flexible micro-supercapacitors with high specific capacitance *Carbon* **125** 308–17
[57] Ye R, Chyan Y, Zhang J, Li Y, Han X, Kittrell C and Tour J M 2017 Laser-induced graphene formation on wood *Adv. Mater.* **29** 1702211